https://doi.org/10.1093/brain/awab319 BRAIN 2022: 145; 729–743 | 729

BRAIN
ORIGINAL ARTICLE

Functional protection in J20/VLW mice: a model of non-demented with Alzheimer's disease neuropathology

Eva Dávila-Bouziguet,[1,2] Arnau Casòliba-Melich,[1,2] Georgina Targa-Fabra,[1,2] Lorena Galera-López,[3] Andrés Ozaita,[3] Rafael Maldonado,[3] Jesús Ávila,[2,4] José M. Delgado-García,[5] Agnès Gruart,[5] Eduardo Soriano[1,2] and Marta Pascual[1,2]

Alzheimer's disease comprises amyloid-β and hyperphosphorylated Tau accumulation, imbalanced neuronal activity, aberrant oscillatory rhythms and cognitive deficits. Non-demented with Alzheimer's disease neuropathology defines a novel clinical entity with amyloid-β and Tau pathologies but preserved cognition. The mechanisms underlying such neuroprotection remain undetermined and animal models of non-demented with Alzheimer's disease neuropathology are currently unavailable.

We demonstrate that J20/VLW mice (accumulating amyloid-β and hyperphosphorylated Tau) exhibit preserved hippocampal rhythmic activity and cognition, as opposed to J20 and VLW animals, which show significant alterations. Furthermore, we show that the overexpression of mutant human Tau in coexistence with amyloid-β accumulation renders a particular hyperphosphorylated Tau signature in hippocampal interneurons. The GABAergic septohippocampal pathway, responsible for hippocampal rhythmic activity, is preserved in J20/VLW mice, in contrast to single mutants.

Our data highlight J20/VLW mice as a suitable animal model in which to explore the mechanisms driving cognitive preservation in non-demented with Alzheimer's disease neuropathology. Moreover, they suggest that a differential Tau phosphorylation pattern in hippocampal interneurons prevents the loss of GABAergic septohippocampal innervation and alterations in local field potentials, thereby avoiding cognitive deficits.

1 Department of Cell Biology, Physiology and Immunology, Institut de Neurociències, Universitat de Barcelona, Barcelona, Spain
2 Centro de Investigación Biomédica en Red sobre Enfermedades Neurodegenerativas (CIBERNED, ISCIII), Spain
3 Laboratory of Neuropharmacology-NeuroPhar, Department of Experimental and Health Sciences, Pompeu Fabra University, Barcelona, Spain
4 Centro de Biología Molecular Severo Ochoa (CSIC-UAM), Neurobiology Laboratory, Madrid, Spain
5 Division of Neurosciences, Pablo de Olavide University, Seville, Spain

Correspondence to: Marta Pascual
Department of Cell Biology, Physiology and Immunology, Institut de Neurociències
Universitat de Barcelona, Barcelona, Spain
E-mail: marpascual@ub.edu

Keywords: Alzheimer's disease; GABAergic neurons; Tau phosphorylation; hippocampus; septohippocampal pathway

Received February 05, 2021. Revised June 19, 2021. Accepted July 28, 2021. Advance access publication August 23, 2021

Abbreviations: CA = cornu ammonis; GAD = glutamic acid decarboxylase; hTau = human Tau protein; LFP = local field potential; MSDB = medial septum and diagonal band of Broca; NDAN = non-demented with Alzheimer's disease neuropathology; P-Tau = hyperphosphorylated Tau protein; PV = parvalbumin; SH = septohippocampal

Introduction

The histopathological hallmarks of Alzheimer's disease include neurodegeneration, extracellular deposits of amyloid-β peptide (i.e. senile plaques) and intracellular neurofibrillary tangles of hyperphosphorylated Tau protein (P-Tau).[1] Moreover, altered neural activity, such as synaptically driven hyperactivity, occurs in mouse models of Alzheimer's disease,[2,3] and functional MRI studies have also revealed hippocampal hyperactivity in asymptomatic individuals at genetic risk of Alzheimer's disease.[4,5] Furthermore, epileptiform activity is more common in individuals with this disease than in controls.[6] Theta and gamma oscillations of local field potentials (LFPs) are reduced in Alzheimer's disease patients and animal models, thereby further indicating an imbalance between excitatory and inhibitory circuits.[7–10] Theta and gamma oscillations are regulated by fast-spiking, parvalbumin (PV)-positive hippocampal interneurons.[11,12] At the circuit level, these cells provide perisomatic inhibition onto glutamatergic pyramidal and granular neurons and regulate spike timing.[13] Consistent with a decrease in PV output in Alzheimer's disease, pyramidal neurons show reduced spontaneous GABAergic currents, and optogenetic stimulation of PV-positive cells improves gamma oscillations and reduces amyloid-β load and P-Tau levels in mouse models of Alzheimer's disease.[14,15] Additional work suggests that loss of GABAergic tone partly underlies network dysfunction in Alzheimer's disease and tauopathies.[16–18]

The medial septum and diagonal band of Broca (MSDB) complex and the nucleus basalis of Meynert innervate the cerebral cortex and the hippocampus. Along with cholinergic fibres, the septohippocampal (SH) pathway consists of another key element, namely the GABAergic SH pathway. This component involves inhibitory long-range projection neurons that terminate specifically on GABAergic hippocampal interneurons,[19,20] which in turn govern the activity of pyramidal neurons. The activation of GABAergic SH neurons results in the selective inhibition of inhibitory interneurons, hence enabling the synchronous activation of a large number of pyramidal neurons.[21,22] Therefore, the GABAergic SH pathway has been proposed to be responsible for producing the correct levels of excitation, as well as regulating synchronous neuronal activity, including theta and gamma oscillations, which are crucial for memory and cognition.[23–26]

Alterations in the GABAergic SH pathway have been associated with Alzheimer's disease. For instance, J20 mice expressing human amyloid precursor protein (hAPP) with Swedish and Indiana mutations of familial Alzheimer's disease[27] present a marked deterioration, manifested as a reduced number and complexity of GABAergic SH axon terminals. This decline also correlates with electrophysiological changes within the hippocampal network.[9,28] Similarly, VLW mice expressing human Tau protein (hTau) with three mutations related to frontotemporal dementia with parkinsonism linked to chromosome 17 (FTDP-17)[29] show a decrease in GABAergic SH innervation.[30] Moreover, VLW mice present epilepsy and $GABA_A$ receptor-mediated hyperexcitability.[31]

Interestingly, individuals presenting the histopathological hallmarks of Alzheimer's disease (namely amyloid-β plaques and P-Tau tangles) without cognitive impairment have been reported.[32–37] This clinical entity, called non-demented with Alzheimer's disease neuropathology (NDAN), is thought to have intrinsic mechanisms conferring neuroprotection against the classical degeneration of Alzheimer's disease. Several factors have been proposed as responsible for this protection, such as increased neurogenesis,[33] increased hippocampal and total brain volume (which could indicate a larger cognitive reserve),[34] neuronal and nuclear hypertrophy,[35] and preservation of the essential elements of the synaptic machinery that are dysfunctional in Alzheimer's disease.[32,36] A differential pattern of cytokine expression, linked to reduced glial activation in human resilience to Alzheimer's disease, together with the absence of soluble P-Tau accumulation in synapses, might contribute to the prevention of neuronal dysfunction in NDAN patients.[38,39] These individuals also have a differential gene expression pattern at the postsynaptic density that differs from that of Alzheimer's disease and control participants and may contribute to the mechanisms that confer synapse protection against Alzheimer's disease.[37] The lack of animal models mimicking NDAN hinders its characterization and identification of the mechanisms involved in preventing cognitive decline.

To assess the synergic or opposing effects of amyloid-β and P-Tau on hippocampal neuron physiology, hippocampal activity rhythms and cognition, we crossed J20 ($hAPP^{Sw,Ind}$) and VLW ($hTau^{VLW}$) mice to generate a double transgenic mouse model with both amyloid-β and Tau pathologies, which are characteristic of Alzheimer's disease. The amyloid-β plaque load in the resulting J20/VLW mice did not differ from that in single transgenic J20 animals. Analysis of Tau phosphoepitopes revealed high levels of Tau phosphorylated at Thr231 (pThr231) and Thr205 (pThr205) in cornu ammonis (CA) 1 pyramidal neurons in J20/VLW mice, similar to VLW animals. In contrast, J20/VLW mice presented higher densities of hippocampal interneurons accumulating pThr205 and pSer262 Tau than VLW animals, thereby indicating an interneuron-specific modulation of Tau phosphorylation by amyloid-β. Surprisingly, GABAergic SH innervation on hippocampal interneurons in J20/VLW mice did not differ from that in control animals. Examination of hippocampal electrophysiology revealed partial recovery of hippocampal theta oscillations in J20/VLW animals, while these oscillations were greatly impaired in J20 and VLW mice. Furthermore, recognition memory deficits associated with amyloid-β accumulation were prevented in the double transgenic mouse model. These data render the J20/VLW mouse line a suitable animal model in which to further study the cognitive preservation in human NDAN participants, and they support the maintenance of the GABAergic system as a mechanism underlying functional hippocampal electrophysiological activity and cognitive neuroprotection in NDAN.

Materials and methods

Animals

A double transgenic mouse line was generated by crossing J20 and VLW lines in a C57BL/6J genetic background. The offspring included double mutant J20/VLW, hemizygous J20, heterozygous VLW and non-transgenic wild-type mice that were used as controls. J20 animals overexpress $hAPP^{Sw,Ind}$, hAPP carrying two familial Alzheimer's disease mutations, namely Swedish (K670N/M671L) and Indiana (V717F), under the control of the platelet-derived

growth factor subunit β promoter.[27] VLW mice overexpress hTau^{VLW}, hTau with four tubulin-binding repeats and three mutations related to FTDP-17 (G272V, P301L and R406W) under the control of the Thy-1 promoter.[29]

For all experiments, *n* denotes the number of animals. Animals were mainly littermates and all of them were derived from the same colony. For the histological procedures, wild-type (8 and 12 months old; *n* = 4–5 per group], J20 (8 and 12 months old; *n* = 4 per group), VLW (8 months old; *n* = 3–4 per group) and J20/VLW (8 and 12 months old; *n* = 4–5 per group) mice were used. For the biochemical analyses, 6–8-month-old wild-type (*n* = 6), J20 (*n* = 2–6), VLW (*n* = 6) and J20/VLW (*n* = 2) mice were used. For the electrophysiological study, 8-month-old wild-type, VLW and J20/VLW mice were used (*n* = 4 per group). For the behavioural tests, 8-month-old wild-type (*n* = 9), J20 (*n* = 6), VLW (*n* = 7) and J20/VLW (*n* = 5) mice were used.

Animals were kept on a 12-h light/dark schedule with access to food and water *ad libitum*. Experimenters were blinded to the genotype of mice until data acquisition was completed. Experiments were performed in accordance with the European Community Council Directive and the National Institute of Health Guide for the Care and Use of Laboratory Animals and were approved by the local ethical committees.

Detection of septohippocampal fibres

Animals were anaesthetized with a 10/1 mixture of Ketolar® (50 mg/ml ketamine chlorhydrate, Parke-Davis)/Rompun® (2% xylidine-thiazine chlorhydrate, Bayer) and stereotaxically injected with an anterograde tracer, 10% biotinylated dextran-amine (BDA; 10 000 MW, Molecular Probes), in the MSDB complex. Each animal received midline injections of the tracer into the MSDB complex at one anteroposterior (AP) level and two dorsoventral (DV) injection sites by iontophoresis. Stereotaxic coordinates in millimetres were (from Bregma): AP 0.7 and DV –3.0 and –3.7.[40] This protocol results in intense BDA labelling in the MSDB complex, which contains the highest proportion of GABAergic SH neurons.[41] After 5–6 days, animals were anaesthetized and perfused with 4% paraformaldehyde in 0.1 M phosphate buffer. Brains were post-fixed for 48 h in 4% paraformaldehyde, cryoprotected in PBS with 30% sucrose, frozen and 30-μm coronal sections were cut and stored in a cryoprotectant solution (30% glycerol, 30% ethylene glycol, 40% 0.1 M phosphate buffer) at –20°C until use.

Immunodetection

Sections from iontophoretically injected animals were processed for double immunodetection of BDA and interneuron or P-Tau markers.[41] Sections were incubated simultaneously with the ABC complex (Vector Laboratories; 1/100) to visualize BDA, and rabbit polyclonal antibodies against PV (Swant®; 1/3000) or glutamic acid decarboxylase isoforms 65 and 67 (GAD, Chemicon International; 1/2000) for interneuron markers, or AT-180 mouse anti-phosphothreonine 231 (Innogenetics; 1/300), T205 rabbit anti-phosphothreonine 205 (Invitrogen™; 1/1000) or S262 rabbit anti-phosphoserine 262 (Invitrogen™; 1/100) antibodies for P-Tau residues. BDA was developed with hydrogen peroxide and diaminobenzidine, nickel ammonium sulphate and cobalt chloride, yielding a black end product in SH fibres. Primary antibodies were visualized by sequential incubation with biotinylated secondary antibodies and the ABC complex (Vector Laboratories). Peroxidase activity was developed with hydrogen peroxide and diaminobenzidine to produce a brown end product. Sections were mounted onto gelatinized slides, dehydrated and coverslipped with Eukitt® (O. Kindler).

To detect pThr231, pThr205, pSer262 Tau or hTau, sections were incubated with AT-180, T205, S262 or HT7 mouse anti-hTau (Invitrogen™; 1/500) antibodies. Subsequent steps were performed as described.

To detect amyloid-β plaques or hAPP, sections were incubated with 3D6 mouse anti-amyloid-β (amino acids 1–5) [obtained from the supernatant of cultured Murine Hybridoma Cell Line, RB96 3D6.32.2.4 (PTA-5130)], American Type Culture Collection; 1/200) or 6E10 mouse anti-amyloid-β and hAPP (amino acids 1–16) (Covance; 1/500) antibodies. Subsequent steps were performed as described.

Analysis of histological sections

Microscopic observations focused on sections corresponding to the medial septum and to dorsal (sections between AP –1.6 and –2.3 mm from Bregma) and ventral (sections between AP –2.9 and –3.4 mm from Bregma) hippocampal levels, following the atlas reported by Paxinos and Franklin.[40]

To estimate the density of hippocampal interneurons and the percentage of these cells contacted by GABAergic SH fibres, the density of interneurons containing GAD, PV, pThr231, pThr205 or pSer262 Tau and the percentage of these receiving BDA-positive pericellular baskets was calculated in distinct regions of the hippocampal area (CA1, CA3 and dentate gyrus) of each section (8-month-old wild-type, J20, VLW and J20/VLW mice and 12-month-old wild-type and J20/VLW mice; *n* = 4–5 animals per group, three sections per animal). The area comprising the hippocampal region of each section was quantified using Fiji software.[42] Because of the large number of GAD-immunopositive cells, several sample areas were selected for each section (8-month-old wild-type, J20, VLW and J20/VLW mice and 12-month-old wild-type and J20/VLW mice; *n* = 4 animals per group, three sections per animal). The selected samples (125-μm wide stripes) contained all hippocampal layers (perpendicularly from the ventricle to the pial surface), and each section included the CA1, the CA3 and the dentate gyrus. Data were represented as density of interneurons per square millimetre and percentage of GAD-, PV-, pThr231, pThr205 or pSer262 Tau-positive cells contacted by GABAergic SH fibres. To assess the complexity of GABAergic SH contacts, synaptic boutons around the soma of GAD-, PV-, pThr231, pThr205 or pSer262 Tau-positive cells were counted in the same sample areas under an optical microscope (Nikon E600, Nikon Corporation), and data were expressed as number of boutons per basket.

To estimate the density of interneurons accumulating pThr231, pThr205 or pSer262 Tau, and to compute the mean grey value of the pThr231 and pThr205 signals in pyramidal neurons, samples immunodetected with AT-180, T205 or S262 antibodies were scanned with a NanoZoomer 2.0HT whole slide imager (Hamamatsu Photonics) at ×20. The density of pThr231, pThr205 and pSer262 Tau-immunopositive interneurons was quantified in distinct regions of the hippocampal area (CA1, CA3 and dentate gyrus) of each section (8-month-old wild-type, J20, VLW and J20/VLW mice; *n* = 4 animals per group, three sections per animal) and data were expressed as density of cells per square millimetre. The cells and area comprising each hippocampal region were quantified using Fiji software.[42] The mean grey value of the pThr231 and pThr205 Tau signals was calculated in 10-mm^2 stripes in matching regions of the pyramidal layer of the CA1 after thresholding the images to exclude background signal (8-month-old VLW and J20/VLW mice; *n* = 3–4 animals per group, three sections per animal) using Fiji software.[42]

To assess the percentage of amyloid-β plaques in the hippocampus, samples immunodetected with 3D6 antibody were scanned with a NanoZoomer 2.0HT whole slide imager (Hamamatsu Photonics) at ×20. The Trainable Weka

Segmentation plugin[43] from Fiji software[42] was applied to the images by using a set of machine-learning algorithms with a collection of image features selected by the user to produce pixel-based segmentations. Images were processed using a macro provided by Sebastién Tosi (Institute for Research in Biomedicine, Barcelona) to identify and quantify amyloid-β plaques (8- and 12-month-old J20 and J20/VLW mice; $n = 4$ animals per group, three sections per animal).

Biochemical extraction

To obtain protein extracts from brain tissue, animals were sacrificed by cervical dislocation and brains were removed. Hippocampal and other cortical regions were dissected and frozen in liquid nitrogen. Frozen tissue was homogenized in lysis buffer (50 mM HEPES, pH 7.5, 150 mM sodium chloride, 1.5 mM magnesium chloride, 1 mM EGTA, 10% glycerol and 1% Triton™ X-100) containing cOmplete™ Mini Protease Inhibitor Cocktail (Roche) and phosphatase inhibitors (10 mM tetrasodium pyrophosphate, 200 μM sodium orthovanadate and 10 mM sodium fluoride). Homogenates were centrifuged at 16 000*g* for 20 min at 4°C, and supernatants were stored at –80°C until use.

Western blot

To remove endogenous immunoglobulins, samples were incubated with 20 μl of protein G beads (GE Healthcare) for 2 h at 4°C, and cleaned supernatants were recovered by centrifugation. Samples were diluted 1:3 with 3× loading buffer (150 mM Tris-HCl, pH 6.8, 300 mM glycerol, 10% β-mercaptoethanol, 3% SDS, 0.075% bromophenol blue) and boiled for 10 min at 95°C. They were then resolved by 10% SDS–PAGE gels and electrotransferred to 0.45-μm nitrocellulose membranes (GE Healthcare). Membranes were incubated with AT-180 (Innogenetics; 1/1000), T205 (Invitrogen™; 1/1000), K9JA rabbit anti-total Tau (DAKO; 1/20 000), and mouse anti-glyceraldehyde 3-phosphate dehydrogenase (GAPDH, Invitrogen™; 1/10 000) primary antibodies. After sequential incubation with HRP-labelled secondary antibodies (DAKO), membranes were developed with ECL™ Western Blotting Detection Reagents (GE Healthcare). For quantification of western blot, a densitometric analysis of protein bands of interest was performed using Gel-Pro Analyzer v.3.1 software (Media Cybernetic) and was normalized for total Tau (K9JA) and the loading control (GAPDH).

Surgery for the chronic recording of hippocampal local field potentials

Mice were anaesthetized with 0.8–3% halothane delivered from a calibrated Fluotec 5 vaporizer (Datex-Ohmeda) at a flow rate of 1–2 l/min oxygen. Animals were implanted with a recording electrode aimed at the ipsilateral stratum radiatum underneath the CA1 area. Stereotaxic coordinates in millimetres were (from Bregma): AP –2.2, lateromedial (LM) 1.2, and DV –1.0 to –1.5.[40] These electrodes were made of 50-μm Teflon-coated tungsten wire (Advent Research Materials Ltd). A bare silver wire (0.1 mm) was affixed to the skull as a ground. Wires were soldered to a 6-pin socket, which was fixed to the skull with the help of two small screws and dental cement.[44]

Recording procedures

The electroencephalographic field activity of the CA1 area was recorded with the help of Grass P511 differential amplifiers. LFP recordings were carried out with the awake animal placed in either a small box (5 × 5 × 5 cm) to prevent walking movements or a large box (20 × 15 × 15 cm) in which the animal could move freely. Recordings were carried out for 20 min, of which up to 5 min of recording free of unwanted artefacts were selected for spectral analysis.

Data analysis of electrophysiological studies

Hippocampal activity was stored digitally on a computer through an analogue/digital converter (CED 1401 Plus, CED) at a sampling frequency of 11–22 kHz and an amplitude resolution of 12 bits. Commercial computer programs (Spike 2 and SIGAVG, CED) were modified to represent recorded LFPs.

The power spectrum of hippocampal LFPs collected was computed with the help of MATLAB v.7.4.0 software (MathWorks), using the fast Fourier transform with a Hanning window, expressed as relative power and averaged across each session. This average was analysed and compared using the wide-band model, considering the following bands: delta (<4 Hz), theta (4.1–8 Hz), alpha (8.1–12 Hz), beta (12.1–26 Hz) and gamma (26.1–100 Hz).[45,46]

Novel object-recognition test

Object-recognition memory was assessed following a protocol previously described.[47] On Day 1, mice were habituated to a V-shaped maze (each corridor measuring 30 cm long × 4.5 cm wide × 15 cm high) for 9 min. On Day 2, two identical objects (familiar objects) were placed at the end of each corridor for 9 min, and the time that the mice spent exploring each object was measured. Twenty-four hours later, one of the familiar objects was replaced by a new object (novel object) (Fig. 1A). The time spent exploring each of the objects was computed to establish a discrimination index, which was calculated as the difference between the time spent exploring the novel object minus the time exploring the familiar object divided by the total exploration time (addition of the time exploring both objects). Object exploration was defined as the orientation of the nose towards the object at a distance of <2 cm. Mice that explored both objects for <10 s or one object for <3 s were excluded from the analysis. A higher discrimination index is considered to reflect greater memory retention for the familiar object. Total exploration time was considered a measure of general activity during the test.

Statistical analysis

Data were processed for statistical analysis with GraphPad Prism 8 (GraphPad Software Incorporated). Data were tested for normal distribution. To examine differences between two experimental groups, an unpaired two-tailed Student's *t*-test or Welch's *t*-test was used when the samples had equal variances or not, respectively. To assess differences between >2 experimental groups, one-way ANOVA was used. *Post hoc* comparisons were performed by Tukey's test or Fisher's LSD test when a significant main effect of one-way ANOVA was revealed. Significance levels were set at $P < 0.05$: $^{*}P < 0.05$, $^{**}P < 0.01$ and $^{***}P < 0.001$. Statistical values of continuously distributed data are presented as mean ± standard error of the mean (SEM) along with all data-points.

Data availability

The data that support the findings of this study are available from the corresponding author on reasonable request.

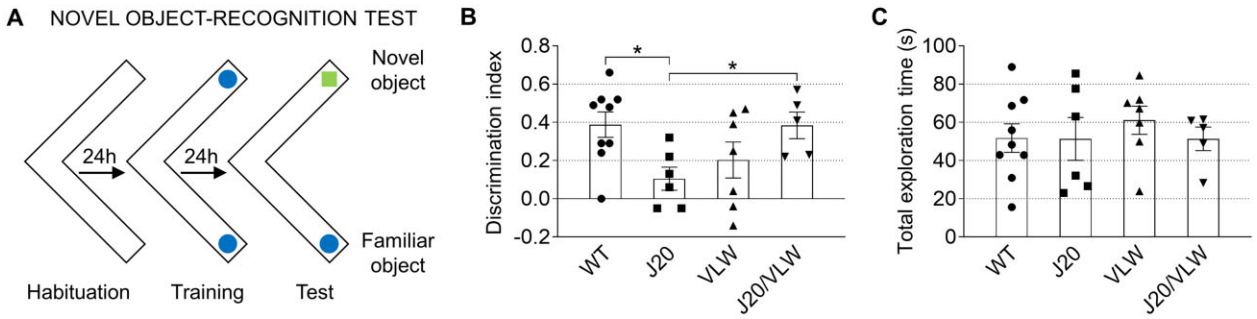

Figure 1 No recognition memory deficits are present in J20/VLW mice. (**A**) Protocol for the novel object recognition test. The time spent exploring each of the objects during the test phase was computed to calculate a discrimination index. (**B**) Discrimination index in the novel object recognition test. A higher discrimination index is considered to reflect greater memory retention for the familiar object. (**C**) Total exploration time in the novel object recognition test was considered a measure of general activity. (**B** and **C**) One-way ANOVA and Fisher's LSD *post hoc*, *$P < 0.05$. 8-month-old wild-type ($n = 9$), J20 ($n = 6$), VLW ($n = 7$) and J20/VLW ($n = 5$) mice. Each dot represents the mean value per animal. Error bars represent SEM.

Results

Cognitive recovery of J20/VLW mice in contrast to J20 animals

J20 and VLW mice show considerable cognitive deficits, mainly in spatial memory.[48–50] To characterize double transgenic J20/VLW mice, which accumulate both amyloid-β and P-Tau, we performed various tests to analyse long-term memory, comparing 8-month-old wild-type, J20, VLW and J20/VLW animals. First, we determined that there were no major differences in either locomotion or anxiety between the four experimental groups (Supplementary Fig. 1). Next, we performed the Y-maze test to study spatial working memory. Our data show that J20/VLW mice presented a higher percentage of correct alternations than J20 and VLW mice (Supplementary Fig. 2). Unexpectedly, alterations in the performance of J20 animals in the novel object recognition test (Fig. 1A), which have been previously described,[48,49] were not present in J20/VLW mice, which showed a behaviour equivalent to that of wild-type mice (Fig. 1B). Surprisingly, these data suggest that the overexpression of mutant hTau, in coexistence with amyloid-β accumulation, protects against the recognition memory deficits associated with amyloid-β. Such specific differences were not related to exploratory behaviour or motility, since total exploration times in the novel object recognition test were similar in the four experimental groups (Fig. 1C).

Hippocampal rhythmic activity preservation in J20/VLW mice

We next analysed the oscillatory activity of hippocampal circuits in 8-month-old behaving wild-type, J20, VLW and J20/VLW mice. Chronically implanted electrodes recorded hippocampal field activity in behaving animals placed in either small or large boxes, to determine the contribution of overt motor activity to the power spectra of the theta and gamma bands (Fig. 2A and B). As previously described,[9] the spectral analysis of LFP recordings showed a clear decrease in the spectral power of the theta band in J20 mice placed in small and large boxes (43% and 38%, respectively) compared to age-matched wild-type animals (Fig. 2C). In addition, a considerable reduction in theta spectral power was present in VLW animals placed in small and large boxes (33% and 42%, respectively). In contrast, J20/VLW mice showed only a slight decrease in theta spectral power when located in small and large boxes (8% and 22%, respectively). We also examined the spectral power of the gamma band (Fig. 2D). In a previous study,[9] we found a 50% reduction in gamma spectral power in J20 animals placed in large and small boxes compared to wild-type mice. The results presented herein demonstrate that the gamma band in VLW animals was equivalent to that of wild-type mice. Interestingly, our data indicate a minor reduction (33%) in this band in J20/VLW mice compared to age-matched wild-type animals. We conclude that both theta and gamma oscillations are rescued in J20/VLW mice. Thus, the coexistence of amyloid-β and P-Tau correlates with preserved hippocampal rhythmic activity.

No changes in amyloid-β accumulation in J20/VLW animals compared to J20 mice

To study changes in amyloid-β accumulation in J20/VLW mice compared to single transgenic J20 animals, we first performed immunodetection with 6E10 antibody (reactive to amino acids 1–16 of amyloid-β and hAPP). No differences were observed in the distribution of 6E10-positive cells or degree of immunoreactivity when comparing the J20 and J20/VLW hippocampus (Supplementary Fig. 3), thus indicating the absence of changes in the level of hAPP expression in double transgenic mice. Subsequently, we measured the concentration of soluble forms of amyloid-β (amino acids 1–42) by ELISA. No differences were observed between 6-month-old J20 and J20/VLW mice (Supplementary Fig. 3). Finally, by immunodetection with 3D6 antibody (which specifically detects amino acids 1–5 of amyloid-β), we analysed the presence of amyloid-β plaques. Our data confirm no changes in the accumulation of amyloid-β plaques in the hippocampus of J20/VLW mice compared to J20 animals at 8 month of age (Fig. 3A–C). Given that there are only a small number of plaques at this maturation stage, we then analysed 12-month-old animals. The percentage of amyloid-β plaques in the hippocampus of 12-month-old J20 and J20/VLW littermates was similar (Fig. 3D–F), suggesting that the cognitive and physiological improvements observed in J20/VLW animals are not a consequence of a reduction in soluble amyloid-β levels or a diminution in amyloid-β plaque load.

Differential Tau phosphorylation signature in hippocampal GABAergic interneurons of J20/VLW mice

Amyloid-β induces Tau phosphorylation both *in vivo* and *in vitro*.[51,52] Therefore, we analysed soluble Tau phosphorylated at Thr231 and Thr205 by western blot of hippocampal and cortical protein extracts from 6–8-month-old wild-type, J20, VLW and J20/VLW mice. Our data show no major changes in the levels of pThr231 Tau between the four experimental groups (Fig. 4A). In contrast, the levels of pThr205 Tau showed a clear

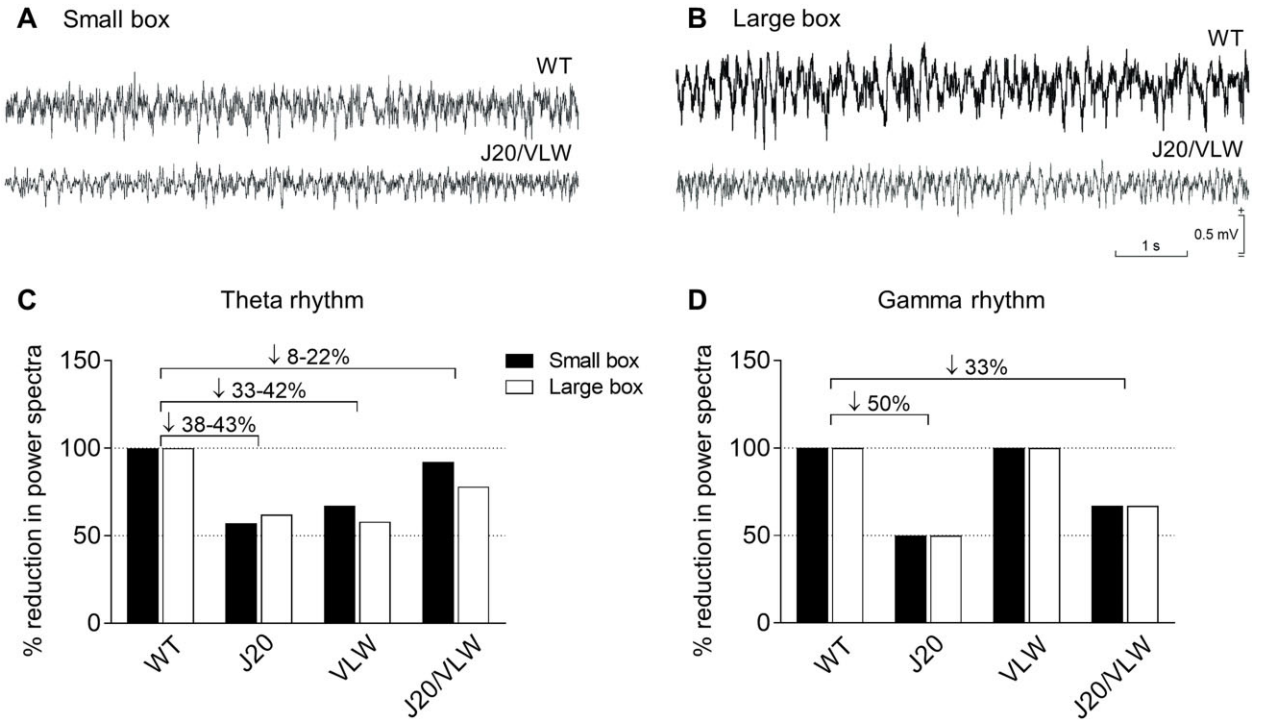

Figure 2 Hippocampal oscillations, which are markedly impaired in J20 and VLW animals, are partially rescued in J20/VLW mice. (**A** and **B**) Representative examples of LFP activity recorded in the CA1 region of the hippocampus of 8-month-old wild-type (WT) and J20/VLW mice placed in either a small (**A**) or a large (**B**) box. (**C** and **D**) Spectral powers were computed from similar records collected from 8-month-old wild-type, J20, VLW and J20/VLW mice. Histograms representing the percentage decrease in spectral power for theta (**C**) and gamma (**D**) bands, comparing J20, VLW and J20/VLW mice to wild-type animals. *n* = 4 animals per group.

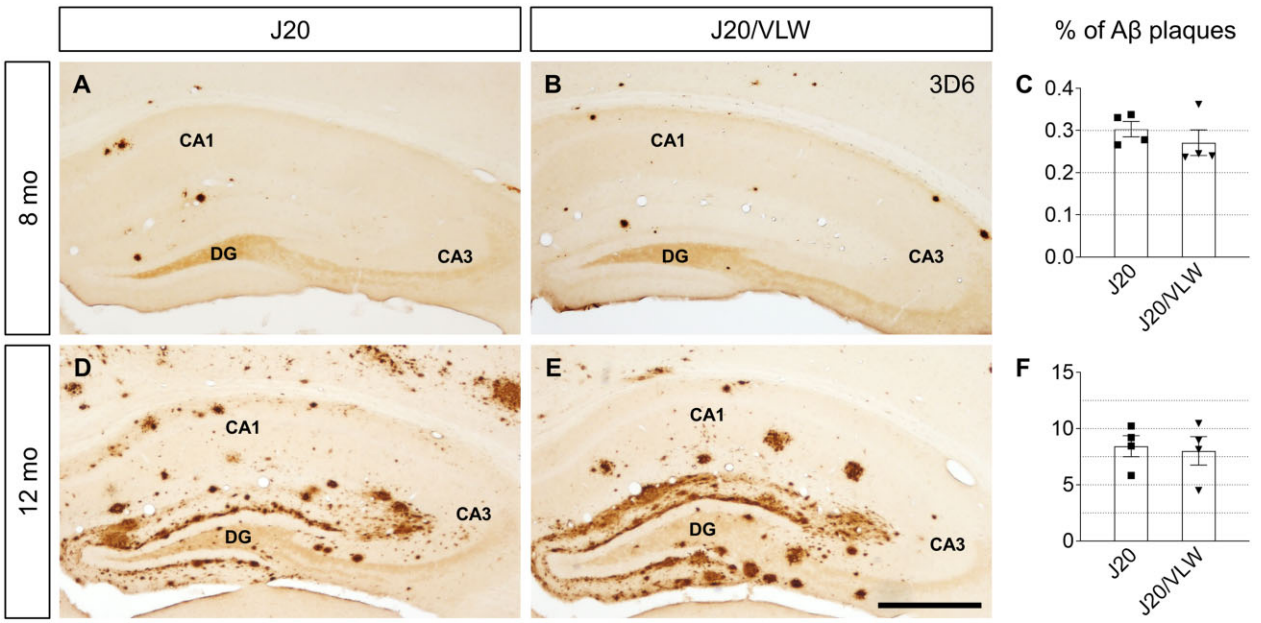

Figure 3 Amyloid-β plaque load of J20/VLW mice is similar to that of J20 animals. Immunodetection of amyloid-β (Aβ) plaques with 3D6 antibody in hippocampal sections from 8- and 12-month-old J20 and J20/VLW mice. (**A**, **B**, **D** and **E**) Accumulation of amyloid-β plaques in the hippocampus of 8- (**A** and **B**) and 12- (**D** and **E**) month-old J20 and J20/VLW mice. (**C** and **F**) Quantification of the percentage of amyloid-β plaques in the hippocampus of 8- (**C**) and 12- (**F**) month-old J20 and J20/VLW animals. (**C** and **F**) Student's *t*-test. *n* = 4 animals per group, three sections per animal. Each dot represents the mean value per animal. Error bars represent SEM. Scale bar = 500 μm.

upwards trend in J20 and J20/VLW mice when compared to wild-type and VLW animals (Fig. 4B), suggesting an effect of amyloid-β on the phosphorylation of Tau at Thr205, as previously described.[53,54]

Next, we examined the pattern of Tau phosphorylation in 8-month-old mice by immunodetection. Our previous data determined that VLW mice overexpress mutant hTau specifically in pyramidal neurons and that phosphorylated hTau in these

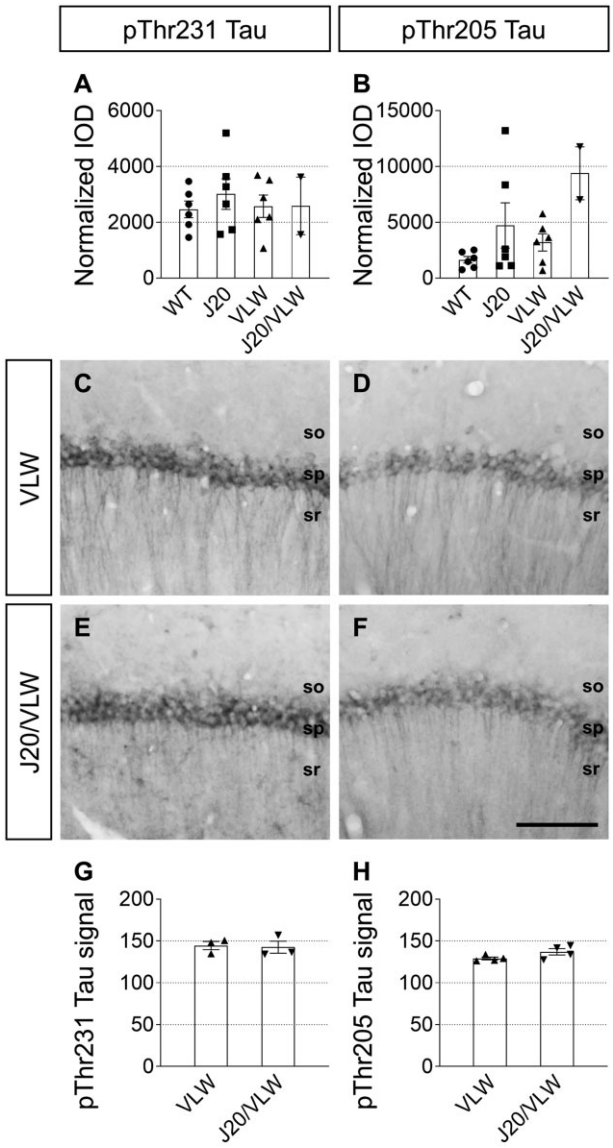

Figure 4 Global levels of pThr231 and pThr205 Tau are not changed in J20/VLW mice. Western blot, immunodetection and quantification of pThr231 and pThr205 Tau. (**A** and **B**) Western blot against pThr231 (**A**) and pThr205 Tau (**B**) in hippocampal and cortical protein extracts from 6–8-month-old wild-type (WT), J20, VLW and J20/VLW mice. (**C–F**) pThr231 (**C** and **E**) and pThr205 (**D** and **F**) Tau accumulation in pyramidal neurons in the CA1 region of the hippocampus of 8-month-old VLW and J20/VLW mice. (**G** and **H**) Quantification of the mean grey value of pThr231 (**G**) and pThr205 (**H**) Tau signal in the pyramidal layer of VLW and J20/VLW animals. (**A** and **B**) One-way ANOVA and Tukey's *post hoc*. $n = 2–6$ animals per group. (**G** and **H**) Student's *t*-test. $n = 3–4$ animals per group, three sections per animal. Each dot represents the mean value per animal. Error bars represent SEM. so = stratum oriens; sp = stratum pyramidale; sr = stratum radiatum. Scale bar = 100 μm. IOD = integrated optical density.

cells induces the phosphorylation of murine Tau in hippocampal interneurons.[54] To analyse the distribution of hTau in J20/VLW hippocampal neurons, we performed immunodetection with HT7 antibody. As in VLW animals, hTau expression in J20/VLW mice was restricted to pyramidal neurons (Supplementary Fig. 4).

Subsequently, we show that there are no changes in the accumulation of Tau phosphorylated at Thr231 or Thr205 in the somatodendritic compartment of pyramidal neurons when comparing VLW and J20/VLW mice (Fig. 4C–F). No differences in the pThr231 and pThr205 Tau signals in the CA1 pyramidal layer were detected between VLW and J20/VLW animals (Fig. 4G and H). No pSer262 Tau was detected in the pyramidal layer of either VLW or J20/VLW mice.

We next compared the distribution and density of interneurons accumulating P-Tau in VLW and J20/VLW mice, as recent data reports the presence of murine pThr231, pThr205 and pSer262 Tau in the somas of hippocampal interneurons in VLW mice.[54] Some hippocampal interneurons located mainly in the stratum oriens of the CA1 accumulated pThr231 Tau both in VLW and J20/VLW mice (Fig. 5A and D). Although no statistical differences in the density of pThr231 Tau-positive interneurons were found between the VLW and J20/VLW hippocampus, a clear upwards trend was observed in the double transgenic mice (Fig. 5G). Subsequently, we examined the density and distribution of pThr205 Tau-positive cells. In agreement with our previous studies,[54] amyloid-β in J20 mice induced an increase in the density of pThr205 Tau-positive hippocampal interneurons in comparison with wild-type mice, and P-Tau accumulation in VLW mice induced a reduction in the density of these interneurons (Fig. 5B and H). The density of pThr205 Tau-positive GABAergic interneurons in J20/VLW mice was higher than in VLW animals, lower than in J20 mice and similar to that of wild-type animals (Fig. 5E and H). Thus, our data indicate that the increase in the density of pThr205 Tau-positive interneurons induced by amyloid-β and the decrease observed in the VLW hippocampus are abolished by the simultaneous presence of amyloid-β and P-Tau in J20/VLW animals (Fig. 5B, E and H). Finally, we show a considerable increase in the density of interneurons accumulating pSer262 Tau in J20/VLW mice compared to VLW animals (Fig. 5C, F and I). This observation suggests a synergic effect of P-Tau and amyloid-β in the induction of Tau phosphorylation at Ser262 in hippocampal interneurons. We thus conclude that the coexistence of amyloid-β and P-Tau in J20/VLW mice confers a particular Tau phosphorylation signature in GABAergic hippocampal interneurons but not in hippocampal pyramidal neurons.

To characterize the interneuron subtypes accumulating P-Tau, we performed double fluorescent immunodetection of pThr231, pThr205 and pSer262 Tau, combined with detection of the interneuron markers PV, calretinin and calbindin, on J20/VLW hippocampal slices. As described in VLW animals, pThr231 Tau accumulated specifically in some PV-positive interneurons throughout the hippocampus (Supplementary Fig. 5A–C), while some PV-, calretinin- and calbindin-positive interneurons scattered in different hippocampal layers and regions accumulated pThr205 and pSer262 Tau (Supplementary Fig. 5D–L). In agreement with previous data in human Alzheimer's disease,[55] only a few PV-positive cells with pThr205 Tau in their soma were present in the J20/VLW hippocampus.

GABAergic septohippocampal pathway preservation in J20/VLW mice

The GABAergic SH pathway is crucial for the activity of hippocampal interneurons and hippocampal physiology, rhythmic activity and cognition.[14,25] Given that the previous data demonstrate the preservation of cognition and hippocampal rhythmic activity in J20/VLW mice and an alteration of the pattern of Tau phosphorylation specifically in interneurons, we next analysed GABAergic SH innervation on interneurons accumulating P-Tau. To map the GABAergic SH pathway, we performed stereotaxic injections of an anterograde tracer (BDA) in the MSDB complex.[9,30,41] By double immunodetection of the tracer and pThr231, pThr205 and pSer262 Tau, we determined the percentage of cells accumulating P-Tau and that are innervated by septal GABAergic fibres, and the

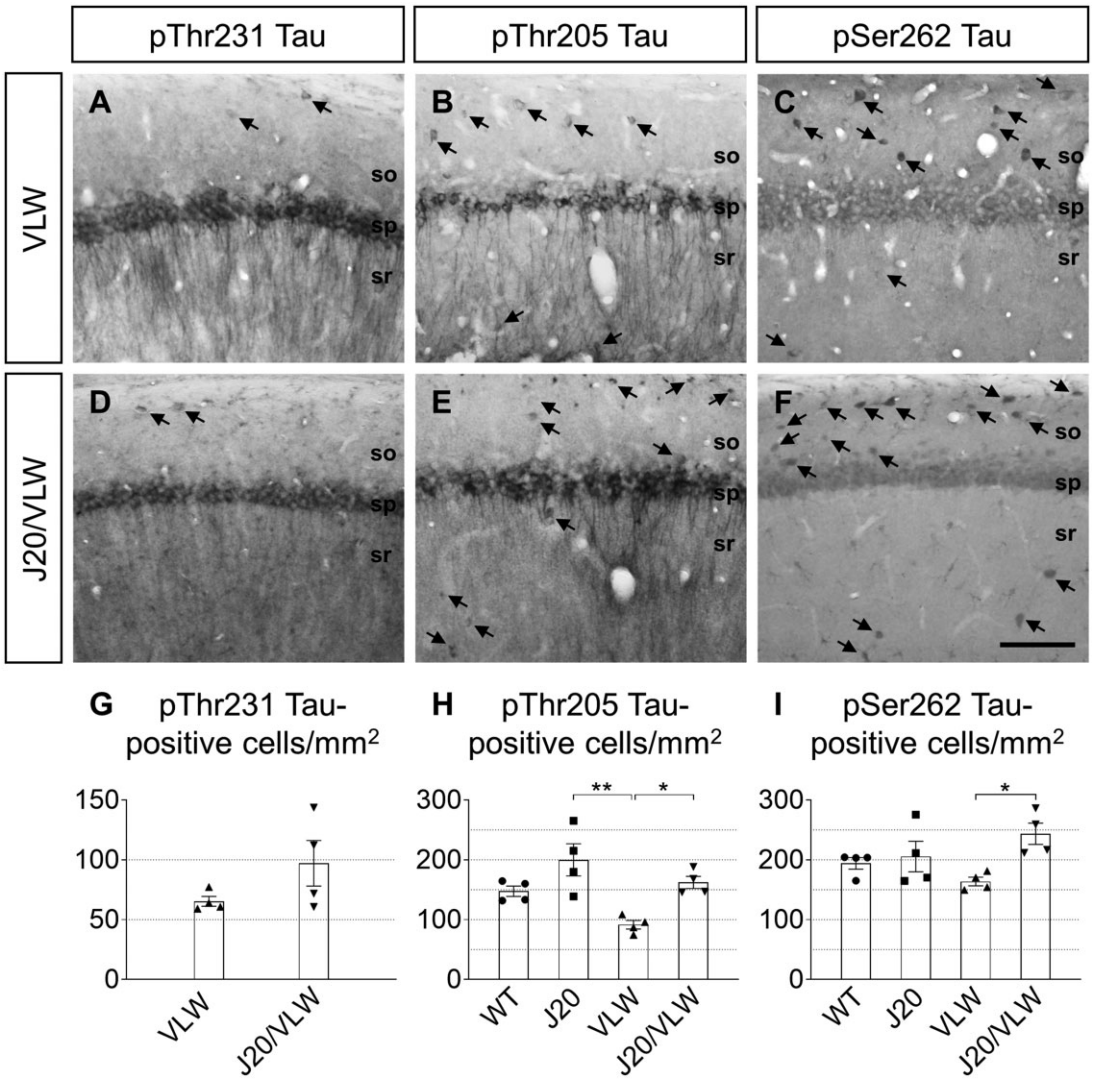

Figure 5 Increased density of hippocampal interneurons accumulating P-Tau in J20/VLW mice, which accumulate amyloid-β peptide, compared to VLW animals. Immunodetection and cell density quantification of pThr231, pThr205 and pSer262 Tau-positive cells in hippocampal sections from 8-month-old wild-type (WT), J20, VLW and J20/VLW mice. (**A–F**) Accumulation of pThr231 (**A** and **D**), pThr205 (**B** and **E**) and pSer262 (**C** and **F**) Tau in hippocampal interneurons (arrows) in the CA1 region of the hippocampus of VLW and J20/VLW mice. (**G**) Density quantification of pThr231 Tau-positive interneurons in the hippocampus of VLW and J20/VLW mice. (**H** and **I**) Density quantification of pThr205 (**H**) and pSer262 (**I**) Tau-positive interneurons in the hippocampus of wild-type, J20, VLW and J20/VLW mice. For (**G**): Welch's *t*-test. (**H** and **I**) One-way ANOVA and Tukey's *post hoc*, $^{*}P < 0.05$, $^{**}P < 0.01$. $n = 4$ animals per group, three sections per animal. Each dot represents the mean value per animal. Error bars represent SEM. so = stratum oriens; sp = stratum pyramidale; sr = stratum radiatum. Scale bar = 100 μm.

complexity of GABAergic SH contacts (number of boutons per cell). Our data indicate that the percentage of pThr205 Tau-positive interneurons contacted by GABAergic SH fibres was significantly decreased in J20 and VLW animals compared to wild-type and J20/VLW mice. Moreover, the complexity of the contacts was also reduced in J20 and VLW mice (Supplementary Fig. 6A–F). In contrast, we found that the percentage of pSer262 Tau-positive interneurons contacted by GABAergic SH fibres and the complexity of the contacts were similar in wild-type, J20, VLW and J20/VLW animals (Supplementary Fig. 6G–L). We then studied GABAergic SH innervation on pThr231 Tau-positive interneurons present in VLW and J20/VLW mice. No differences in either the percentage of contacted pThr231 Tau-positive interneurons or the complexity of the contacts were detected between VLW and J20/VLW animals (Supplementary Fig. 6M–P).

Thereafter, we studied whether the GABAergic SH network is preserved in J20/VLW mice by double immunodetection of the tracer BDA and interneuron markers. In agreement with our previous studies,[9,30] single transgenic J20 and VLW mice showed a significant reduction in the percentage of GABAergic hippocampal interneurons (GAD-immunopositive) innervated by GABAergic SH fibres, respectively, compared to wild-type animals (Fig. 6G). Also, both groups showed a decrease in the complexity of GABAergic SH synaptic contacts on GAD-positive hippocampal cells (Fig. 6H).[9] These findings suggest that the impairment of GABAergic SH innervation, which modulates hippocampal network activity, may be linked to the cognitive deficits present in J20 and VLW mice.[9,30] We subsequently characterized the GABAergic SH pathway in J20/VLW animals. Neither the distribution nor percentage of GAD-positive neurons contacted by septal GABAergic fibres, nor the complexity of the GABAergic SH contacts were altered in 8-month-old J20/VLW mice compared to wild-type animals (Fig. 6). We next studied GABAergic SH innervation on PV-positive hippocampal interneurons in J20/VLW animals, the hippocampal interneuron

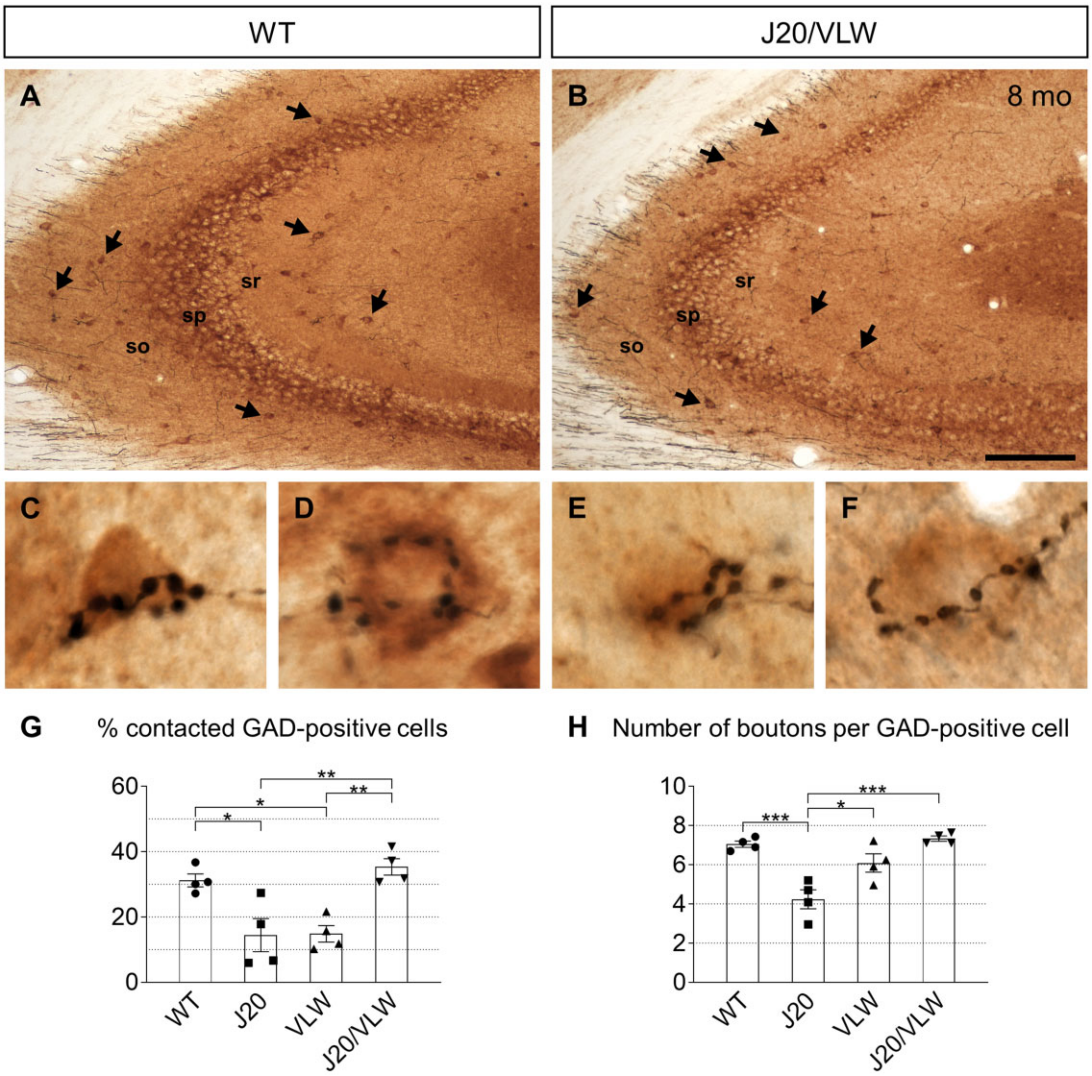

Figure 6 GABAergic SH innervation on GAD-positive cells is preserved in 8-month-old J20/VLW mice. Double immunodetection of GABAergic SH fibres and GAD-positive cells in hippocampal sections from 8-month-old wild-type (WT) and J20/VLW mice. (**A** and **B**) GABAergic SH fibres contacting GAD-positive cells (arrows) in the CA3 region of wild-type (**A**) and J20/VLW (**B**) mice. (**C–F**) GABAergic SH baskets forming synaptic boutons (black) on the soma of GAD-positive cells (brown) in wild-type (**C** and **D**) and J20/VLW (**E** and **F**) mice. (**G** and **H**) Quantification of the percentage of GAD-positive cells contacted by GABAergic SH fibres (**G**) and the complexity of GABAergic SH contacts (**H**) in wild-type, J20, VLW and J20/VLW mice. (**G** and **H**) One-way ANOVA and Tukey's *post hoc*, $^{*}P < 0.05$, $^{**}P < 0.01$, $^{***}P < 0.001$. $n = 4$ animals per group, three sections per animal. Each dot represents the mean value per animal. Error bars represent SEM. so = stratum oriens; sp = stratum pyramidale; sr = stratum radiatum. Scale bars = 150 μm (**A** and **B**), 10 μm (**C–F**).

population most affected by the loss of GABAergic SH innervation in J20 and VLW mice.[9,30] These two groups exhibited a dramatic reduction in the percentage of PV-positive cells contacted by GABAergic SH fibres. Moreover, the complexity of the GABAergic SH synaptic contacts on these cells was diminished in both J20 and VLW mice (Fig. 7G and H).[9,30] In contrast, the distribution and the percentage of PV-containing interneurons contacted by GABAergic SH fibres were spared in J20/VLW mice, and only a slight decrease in the complexity of the GABAergic SH contacts on PV-positive cells occurred (Fig. 7).

To determine whether the improvement in the GABAergic SH innervation in J20/VLW animals is due to a permanent recovery or a delay in the impairment of the GABAergic SH pathway, we analysed 12-month-old mice. Neither a reduction in the percentage of GAD- and PV-positive neurons contacted by GABAergic SH fibres nor in the number of synaptic boutons per GAD- and PV-positive cell was observed in 12-month-old J20/VLW mice, compared to age-matched wild-type animals (Fig. 8).

These data indicate that the maintenance of correct GABAergic SH innervation in J20/VLW mice may contribute to the preservation of cognitive and physiological functions in this double transgenic mouse model. Our findings also suggest that the presence of Tau with a specific phosphorylation pattern, together with amyloid-β accumulation, in J20/VLW mice confers neuroprotection against the GABAergic SH denervation associated with individual amyloid-β and P-Tau pathologies.

To assess the GABAergic cell population in J20/VLW animals, we analysed the density and distribution of hippocampal and septal GABAergic neurons in 8- and 12-month-old mice by immunodetection. The distribution and density of hippocampal GABAergic neurons in J20/VLW mice were similar to those of wild-type counterparts. GAD-positive cells were located throughout distinct

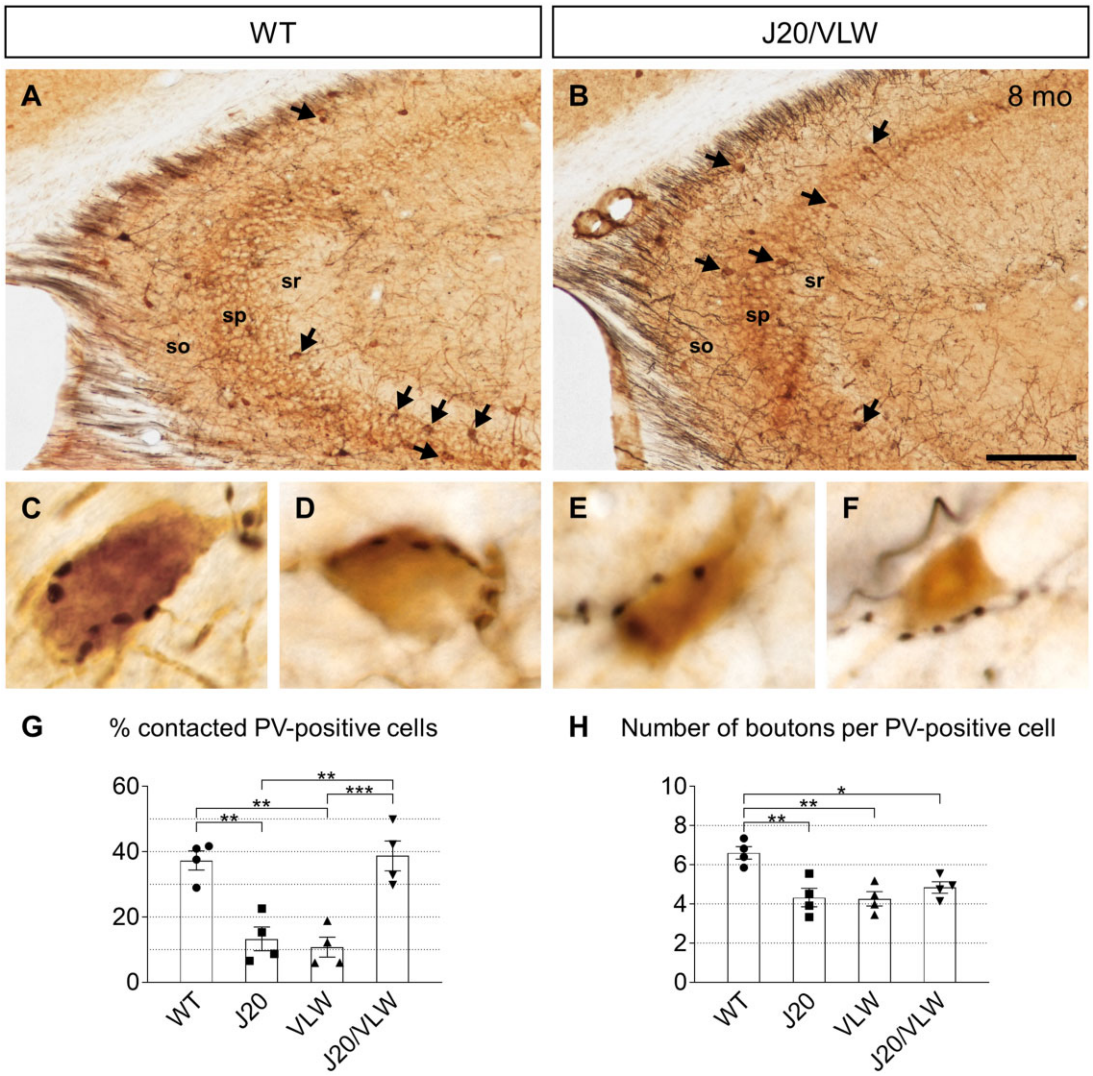

Figure 7 GABAergic SH innervation on PV-positive cells is preserved in 8-month-old J20/VLW mice. Double immunodetection of GABAergic SH fibres and PV-positive cells in hippocampal sections from 8-month-old wild-type (WT) and J20/VLW mice. (**A** and **B**) GABAergic SH fibres contacting PV-positive cells (arrows) in the CA3 region of wild-type (**A**) and J20/VLW (**B**) mice. (**C–F**) GABAergic SH baskets forming synaptic boutons (black) on the soma of PV-positive cells (brown) in wild-type (**C** and **D**) and J20/VLW (**E** and **F**) mice. (**G** and **H**) Quantification of the percentage of PV-positive cells contacted by GABAergic SH fibres (**G**) and the complexity of GABAergic SH contacts (**H**) in wild-type, J20, VLW and J20/VLW mice. (**G** and **H**) One-way ANOVA and Tukey's *post hoc*, $^{*}P < 0.05$, $^{**}P < 0.01$, $^{***}P < 0.001$. $n = 4$ animals per group, three sections per animal. Each dot represents the mean value per animal. Error bars represent SEM. so = stratum oriens; sp = stratum pyramidale; sr = stratum radiatum. Scale bars = 150 μm (**A** and **B**), 10 μm (**C–F**).

layers and areas of the hippocampus (Supplementary Fig. 7A–D). Examination of the PV-positive subtype of interneurons revealed no alterations in either their distribution or density in the J20/VLW hippocampus (Supplementary Fig. 7E–H).

Finally, we studied the GABAergic SH neurons in the septal region by PV immunodetection. The distribution and density of PV-positive cells were preserved in the J20/VLW MSDB complex, compared to age-matched wild-type animals (Supplementary Fig. 8). We conclude that J20/VLW mice do not show an altered distribution or loss of septal and hippocampal GABAergic neurons.

Discussion

Growing evidence indicates that Tau and amyloid-β have opposing effects on neuronal excitability and circuit activity.[56,57] However, the coexistence of Tau- and amyloid-related pathologies has been proposed to act synergistically to impair neural circuit function, and recent studies suggest that Tau has a dominating effect over amyloid-β.[56,57] Moreover, Tau appears to be required for amyloid-β-induced toxicity and endogenous Tau reduction has been shown to improve cognitive deficiencies in J20 mice.[58,59] Conversely, the phosphorylation of Tau at Thr205 inhibits neurotoxicity.[53] A major finding of the present study is that the alterations in theta and gamma rhythms and cognitive deficits observed in single transgenic J20 and VLW animals are not present in J20/VLW mice. Thus, besides displaying amyloid-β and P-Tau pathologies, J20/VLW mice are protected against cognitive and electrophysiological impairments. This finding points J20/VLW mice as a model of NDAN, in which to investigate the fine mechanisms that mediate this relevant clinical entity. Our subsequent analyses suggest that the simultaneous presence of Tau phosphorylated at specific residues in hippocampal interneurons and of amyloid-β accumulation preserves hippocampal function in the double transgenic mouse model by maintaining a functional GABAergic SH pathway.

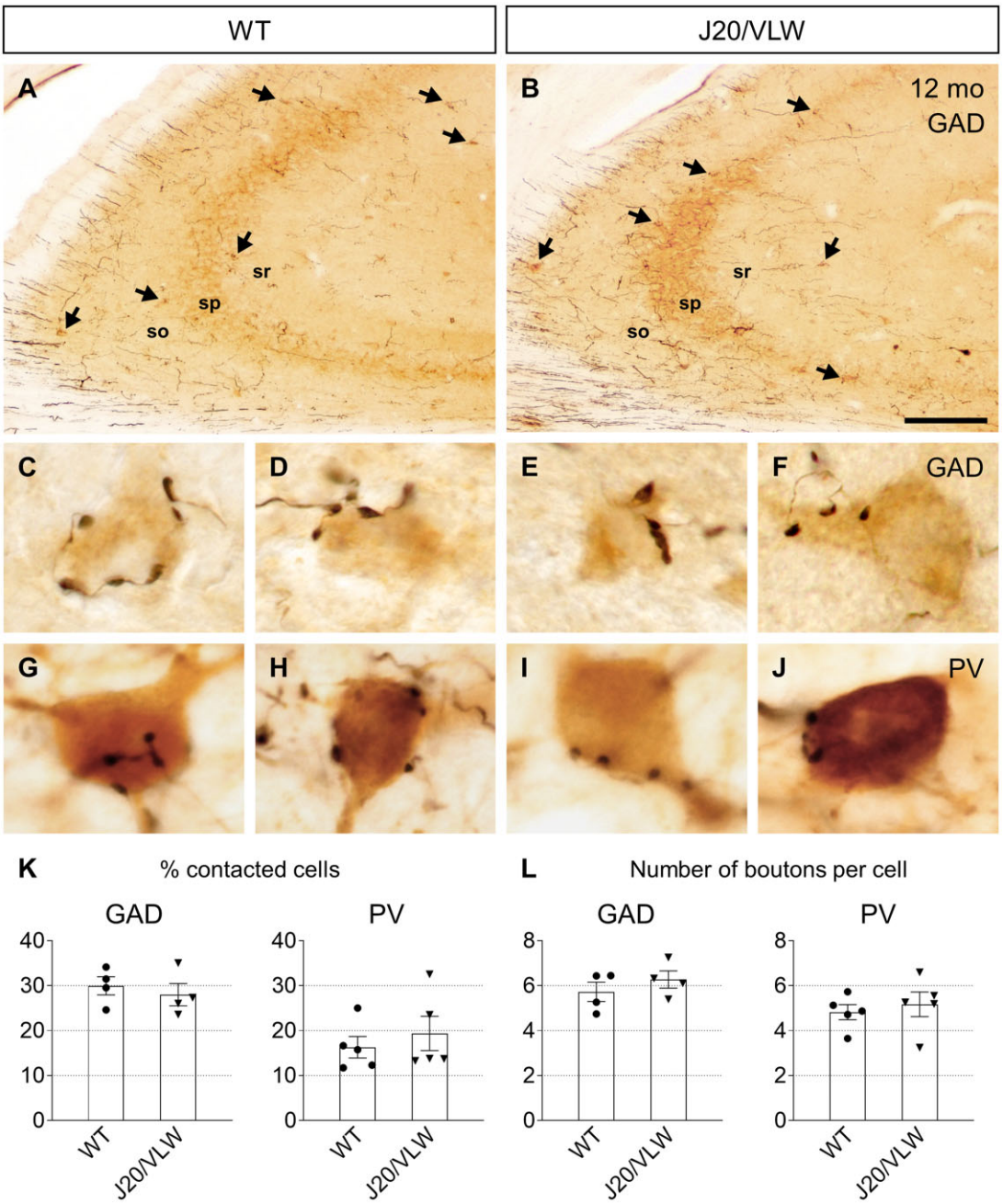

Figure 8 No alterations in GABAergic SH innervation are observed in 12-month-old J20/VLW mice. Double immunodetection of GABAergic SH fibres and GAD- or PV-positive cells in hippocampal sections from 12-month-old wild-type (WT) and J20/VLW mice. (**A** and **B**) GABAergic SH fibres contacting GAD-positive cells (arrows) in the CA3 region of wild-type (**A**) and J20/VLW (**B**) mice. (**C–F**) GABAergic SH baskets forming synaptic boutons (black) on the soma of GAD-positive cells (brown) in wild-type (**C** and **D**) and J20/VLW (**E** and **F**) mice. (**G–J**) GABAergic SH baskets forming synaptic boutons (black) on the soma of PV-positive cells (brown) in wild-type (**G** and **H**) and J20/VLW (**I** and **J**) mice. (**K** and **L**) Quantification of the percentage of GAD- and PV-positive cells contacted by GABAergic SH fibres (**K**) and the complexity of GABAergic SH contacts (**L**) in wild-type and J20/VLW mice. (**K** and **L**) Student's *t*-test. $n = 4–5$ animals per group, three sections per animal. Each dot represents the mean value per animal. Error bars represent SEM. so = stratum oriens; sp = stratum pyramidale; sr = stratum radiatum. Scale bars = 150 μm (**A** and **B**), 10 μm (**C–J**).

While amyloid-β may cause Tau phosphorylation and Tau may increase amyloid-β toxicity, there are conflicting lines of evidence as to whether Tau leads to an increase in amyloid deposition. Certain APP/Tau mice overexpressing hAPP^{Sw} together with hTau P301L (JNPL3/Tg2576 and APP23/B6P301L) show no differences in amyloid-β plaque load compared to single transgenic hAPP^{Sw} mice.[60,61] However, 16-month-old Tg2576/VLW mice displayed enhanced amyloid deposition.[62] Our data reveal no changes in soluble amyloid-β or amyloid-β deposition in J20/VLW mice compared to J20 animals.

Previous studies demonstrated that amyloid-β increases Tau phosphorylation.[63–65] No major changes in the levels of soluble pThr231 Tau were detected in the four experimental groups analysed. In contrast, the levels of pThr205 Tau showed a clear upwards trend in J20 and J20/VLW mice when compared to wild-type and VLW animals. This observation suggests an effect of

amyloid-β on Tau phosphorylation at Thr205, as previously described.[53,54] Also, we did not detect changes in the levels of Tau phosphorylation at either Thr231 or Thr205 in hippocampal pyramidal neurons when comparing VLW and J20/VLW mice, or at pSer262 Tau, which is absent in pyramidal neurons in both animal models. In addition, P-Tau mislocalization to the somatodendritic compartment of pyramidal neurons described previously in VLW mice[29,30,54] occurred in the J20/VLW hippocampus.

Thus, we conclude that the cognitive preservation observed in J20/VLW animals is not due to a reduction in amyloid-β load or to changes in the levels of P-Tau in pyramidal neurons.

In addition to the presence of P-Tau in pyramidal neurons,[66,67] the somas of hippocampal interneurons accumulate P-Tau in control and pathological conditions.[54] As in hAPP^{Sw}/VLW mice,[65] our data indicate that the presence of amyloid-β enhanced Tau microtubule-binding domain phosphorylation at non-proline directed phosphorylation sites such as Ser262 in J20/VLW interneurons in comparison to VLW mice. These findings reveal that amyloid-β facilitates Tau phosphorylation at these sites specifically in GABAergic neurons. The phosphorylation of Tau at Ser262 induces its detachment from microtubules.[68] Moreover, it has been reported that amyloid-β induction of pThr231 Tau is dependent on pSer262.[68] Thus, the clear upwards trend in the density of pThr231 Tau-positive interneurons in J20/VLW mice may result from the increased number of pSer262 Tau-positive interneurons in these animals. Taken together, these data suggest that, in the J20/VLW hippocampus, the increase in Tau phosphorylated at both Ser262 and Thr231 in GABAergic neurons facilitates the somatic localization of Tau, thereby favouring a novel function of this protein in the soma of hippocampal interneurons in this mouse model.

Amyloid-β species cause synaptic loss and dysfunction in both glutamatergic and GABAergic synapses.[9,69] We previously described that amyloid-β accumulation in J20 mice and presence of P-Tau in VLW animals induce abnormal GABAergic SH innervation in these two animal models.[9,30] Our results indicate that J20/VLW mice show a correct GABAergic SH innervation, thereby suggesting that the presence of P-Tau together with amyloid-β accumulation in J20/VLW mice protects against the GABAergic SH denervation associated with amyloid-β and P-Tau separately. Our findings also confirm a permanent effect since no alterations were observed in either 8- or 12-month-old J20/VLW animals. No changes in amyloid-β load or P-Tau accumulation and mislocalization in pyramidal neurons occurred in J20/VLW animals compared to J20 or VLW mice, respectively. Therefore, our findings suggest that the maintenance of correct GABAergic SH innervation in J20/VLW mice is due to the specific pattern of Tau phosphorylation in hippocampal interneurons. In this regard, our data indicate that GABAergic SH innervation is preserved on interneurons accumulating pThr205 Tau in J20/VLW mice, contrary to what is observed in J20 and VLW mice. Conversely, our results regarding pSer262 and pThr231 Tau support the notion that Tau phosphorylated at a single residue in the distinct experimental groups does not have a direct effect on GABAergic SH innervation. This observation would thus support the notion that combined phosphorylation at particular residues of Tau in hippocampal interneurons provides the underlying basis for the maintenance of this pathway.

Tau may participate in the dynamic regulation of $GABA_A$ receptor trafficking at inhibitory synapses through the scaffolding protein gephyrin, which is directly linked to the cytoskeleton.[70] By regulating the clustering of this receptor, gephyrin controls GABAergic synaptic activity and, therefore, inhibitory transmission.[71] Also, it has been described that glycogen synthase kinase 3β (GSK3β), a major Tau kinase activated by amyloid-β, regulates GABAergic synapse formation via the phosphorylation of gephyrin.[72,73]

Further research is required to gain a full understanding of the molecular mechanisms by which a distinct pattern of Tau phosphorylation modulates the function of GABAergic neurons. However, one hypothesis is that GSK3β activation by amyloid-β induces both an increase in P-Tau in the soma of GABAergic interneurons and the phosphorylation of gephyrin, thereby contributing to $GABA_A$ receptor clustering and thus preserving the GABAergic SH synaptic contacts on hippocampal interneurons and stabilizing inhibitory synaptic activity.

Our previous data indicated that impaired GABAergic SH innervation in J20 mice correlates with altered patterns of neuronal hippocampal activity and with internal processes related to operant rewards. Spectral analysis showed a clear decrease in the spectral power of theta and gamma bands in J20 mice, compared to age-matched wild-type animals.[9,28] Furthermore, VLW animals overexpressing mutant hTau display hyperexcitability in the absence of amyloid-β, along with alterations in the GABAergic SH pathway.[30,31] Here we demonstrate a considerable reduction in theta spectral power in VLW animals. In contrast, J20/VLW mice showed only a slight decrease in the spectral power of theta and gamma bands. It has been proposed that the GABAergic SH pathway regulates oscillatory activity, particularly through the recruitment of hippocampal interneurons. The main targets of the GABAergic SH fibres are the axo-axonic and basket PV-positive neurons, which regulate the firing of a large number of pyramidal neurons, hence leading to the generation of oscillatory activity in the range of the theta and gamma frequencies. Overall, our data indicate that, in contrast to the major alterations in theta and gamma rhythms in single transgenic J20 and VLW animals, J20/VLW mice show only minor alterations, pointing to a correlation between preserved GABAergic SH innervation and proper hippocampal rhythmic activity.

The present study explores the relevance of correct GABAergic SH innervation and electrophysiological preservation for the cognitive state of J20/VLW animals. Our results indicate that the simultaneous presence of amyloid-β and P-Tau reverses the cognitive impairment observed in J20 and VLW mice. As described in Alzheimer's disease and some animal models of this pathology,[8,10,16] J20 and VLW animals displayed an imbalance between excitatory and inhibitory circuits associated with hyperexcitability and cognitive deficits. In contrast, J20/VLW animals showed no major alterations in theta and gamma hippocampal rhythms, thereby suggesting a correct excitation/inhibition balance, probably modulated by GABAergic SH fibres and, therefore, by correct hippocampal GABAergic function. Our results reveal no cognitive deficits in J20/VLW animals and point to a correlation between correct GABAergic synaptic function and cognition.

Nevertheless, further studies are needed to confirm the causal role of GABAergic SH pathway preservation in the prevention of cognitive impairment. An interesting experiment to investigate this question would be the intervention to manipulate GABAergic SH pathway activity in J20/VLW mice. This paradigm would allow ascertaining whether either blocking or stimulating the GABAergic SH pathway results in the development of cognitive deficits in our double transgenic model. Similar experiments injecting amyloid-β in the medial septum demonstrated dramatic reductions of hippocampal theta spectral power and significant impairment of memory retention.[74,75] Conversely, the opposite paradigm has also been tested, and it proved that direct optogenetic stimulation of PV-positive GABAergic SH neurons rescues memory impairment in J20 mice.[14] Moreover, indirect manipulation of the medial septum by injecting amyloid-β in the hippocampus, which would be a situation similar to that of J20 mice, demonstrated a significant reduction in the firing rate of GABAergic SH neurons, theta spectral power and recognition memory.[76]

Several research groups have recently described individuals presenting amyloid-β plaques and P-Tau tangles in the absence of cognitive impairment.[32–37] These NDAN participants are thought to have intrinsic mechanisms conferring protection against Alzheimer's disease-associated dementia.

A full understanding of the mechanisms underlying cognitive neuroprotection in the presence of both amyloid-β and P-Tau pathological traits could have a major impact on the design of therapeutic strategies aimed at preventing cognitive decline in patients of Alzheimer's disease. A major factor proposed as responsible for this protection is the preservation of the synaptic machinery that normally degenerates in Alzheimer's disease.[32,36,37] In this regard, we propose that the simultaneous presence of amyloid-β and Tau with a specific phosphorylation pattern in J20/VLW mice confers protection against the synaptotoxic effects of pathogenic oligomers, as seen in NDAN individuals, or triggers a differential pattern of gene expression that protects synaptic structure and function. Our results also point to the preservation of the GABAergic network as a possible factor underlying the recovery of cognitive and physiological deficits in J20/VLW mice. It is worth noting that the studies on NDAN subjects focus on glutamatergic synapses.[32,36,37] Therefore, it would be of interest to analyse the state of GABAergic synapses in NDAN individuals to shed light on potential commonalities shared with J20/VLW mice.

Consistently, post-mortem neuropathological examination and brain imaging studies have revealed cell loss and volume reductions in the nucleus basalis of Meynert and MSDB complex of the basal forebrain in Alzheimer's disease,[77–80] and it is unknown whether NDAN also presents these features. However, to the best of our knowledge, the state of the GABAergic SH pathway in humans has not been studied to date. Our present data, together with the imbalance between excitatory and inhibitory circuits and in the GABAergic network, and oscillatory dysfunctions recurrently associated to Alzheimer's disease,[3–10,16,17] highlight the relevance of analysing the GABAergic SH pathway in humans.

Taken together, our findings suggest that the differential Tau phosphorylation pattern in hippocampal interneurons of J20/VLW mice protects against the loss of GABAergic SH innervation, thereby preventing alterations in LFPs and, subsequently, hindering cognitive deficits. These data support a new role of P-Tau in the maintenance of the GABAergic SH network and hippocampal GABAergic activity and indicate the potential of P-Tau regulation in GABAergic neurons as a therapeutic target in Alzheimer's disease. Finally, we propose the double transgenic mouse line generated herein as a suitable animal model in which to study the cognitive preservation in NDAN participants and to open up new therapeutic strategies to treat Alzheimer's disease-associated dementia.

Acknowledgements

The authors thank the personnel of the Advanced Optical Microscopy Facility at the Scientific and Technological Centers of the University of Barcelona for support, Alba Vílchez-Acosta for technical help and the personnel of the Histopathology Facility of the Institute for Research in Biomedicine for assistance.

Funding

This work was supported by funds from the Ministry of Economy and Competitiveness (SAF2016-76340-R) and the Ministry of Science, Innovation and Universities (PID2019-106764RB-C21/AEI/10.13039/501100011033) to E.S. and (RTI2018-099282-B-I00) to A.O., from the Ministry of Economy, Industry and Competitiveness (BFU2017-82375-R) to A.G. and J.M.D.-G; by the María de Maeztu Unit of Excellence awarded to the Institute of Neurosciences of the University of Barcelona (MDM-2017–0729, Ministry of Science, Innovation and Universities); by an FPU grant from the Ministry of Education, Culture and Sport (FPU2016-07395) awarded to E.D.-B., and by an FPI grant from the Ministry of Economy, Industry and Competitiveness (BES-2016–077950) awarded to L.G.-L.

Competing interests

The authors report no competing interests.

Supplementary material

Supplementary material is available at *Brain* online.

References

1. Kametani F, Hasegawa M. Reconsideration of amyloid hypothesis and tau hypothesis in Alzheimer's disease. *Front Neurosci*. 2018;12:25.
2. Busche MA, Chen X, Henning HA, et al. Critical role of soluble amyloid-β for early hippocampal hyperactivity in a mouse model of Alzheimer's disease. *Proc Natl Acad Sci U S A*. 2012; 109(22):8740–8745.
3. Palop JJ, Chin J, Roberson ED, et al. Aberrant excitatory neuronal activity and compensatory remodeling of inhibitory hippocampal circuits in mouse models of Alzheimer's disease. *Neuron*. 2007;55(5):697–711.
4. Bookheimer SY, Strojwas MH, Cohen MS, et al. Patterns of brain activation in people at risk for Alzheimer's disease. *N Engl J Med*. 2000;343(7):450–456.
5. Reiman EM, Quiroz YT, Fleisher AS, et al. Brain imaging and fluid biomarker analysis in young adults at genetic risk for autosomal dominant Alzheimer's disease in the presenilin 1 E280A kindred: A case-control study. *Lancet Neurol*. 2012;11(12): 1048–1056.
6. Horváth A, Szűcs A, Barcs G, Noebels JL, Kamondi A. Epileptic seizures in Alzheimer disease. *Alzheimer Dis Assoc Disord*. 2016; 30(2):186–192.
7. Mably AJ, Colgin LL. Gamma oscillations in cognitive disorders. *Curr Opin Neurobiol*. 2018;52:182–187.
8. Palop JJ, Mucke L. Network abnormalities and interneuron dysfunction in Alzheimer disease. *Nat Rev Neurosci*. 2016;17(12): 777–792.
9. Rubio SE, Vega-Flores G, Martínez A, et al. Accelerated aging of the GABAergic septohippocampal pathway and decreased hippocampal rhythms in a mouse model of Alzheimer's disease. *FASEB J*. 2012;26(11):4458–4467.
10. Verret L, Mann EO, Hang GB, et al. Inhibitory interneuron deficit links altered network activity and cognitive dysfunction in Alzheimer model. *Cell*. 2012;149(3):708–721.
11. Buzsáki G. Theta oscillations in the hippocampus. *Neuron*. 2002; 33(3):325–340.
12. Sohal VS, Zhang F, Yizhar O, Deisseroth K. Parvalbumin neurons and gamma rhythms enhance cortical circuit performance. *Nature*. 2009;459(7247):698–702.
13. Amilhon B, Huh CYL, Manseau F, et al. Parvalbumin interneurons of hippocampus tune population activity at theta frequency. *Neuron*. 2015;86(5):1277–1289.
14. Etter G, van der Veldt S, Manseau F, Zarrinkoub I, Trillaud-Doppia E, Williams S. Optogenetic gamma stimulation rescues memory impairments in an Alzheimer's disease mouse model. *Nat Commun*. 2019;10(1):5322.

15. Iaccarino HF, Singer AC, Martorell AJ, et al. Gamma frequency entrainment attenuates amyloid load and modifies microglia. *Nature*. 2016;540(7632):230–235.
16. Ambrad Giovannetti E, Fuhrmann M. Unsupervised excitation: GABAergic dysfunctions in Alzheimer's disease. *Brain Res*. 2019; 1707:216–226.
17. Busche MA, Kekuš M, Adelsberger H, et al. Rescue of long-range circuit dysfunction in Alzheimer's disease models. *Nat Neurosci*. 2015;18(11):1623–1630.
18. Shimojo M, Takuwa H, Takado Y, et al. Selective disruption of inhibitory synapses leading to neuronal hyperexcitability at an early stage of tau pathogenesis in a mouse model. *J Neurosci*. 2020;40(17):3491–3501.
19. Freund TF, Antal M. GABA-containing neurons in the septum control inhibitory interneurons in the hippocampus. *Nature*. 1988;336(6195):170–173.
20. Gulyás AI, Görcs TJ, Freund TF. Innervation of different peptide-containing neurons in the hippocampus by GABAergic septal afferents. *Neuroscience*. 1990;37(1):31–44.
21. Freund TF, Gulyás AI. Inhibitory control of GABAergic interneurons in the hippocampus. *Can J Physiol Pharmacol*. 1997;75(5): 479–487.
22. Tóth K, Freund TF, Miles R. Disinhibition of rat hippocampal pyramidal cells by GABAergic afferents from the septum. *J Physiol*. 1997;500 (Pt 2) (2):463–474.
23. Colgin LL, Moser EI. Gamma oscillations in the hippocampus. *Physiology*. 2010;25(5):319–329.
24. Gangadharan G, Shin J, Kim S-W, et al. Medial septal GABAergic projection neurons promote object exploration behavior and type 2 theta rhythm. *Proc Natl Acad Sci U S A*. 2016;113(23): 6550–6555.
25. Hangya B, Borhegyi Z, Szilagyi N, Freund TF, Varga V. GABAergic neurons of the medial septum lead the hippocampal network during theta activity. *J Neurosci*. 2009;29(25):8094–8102.
26. Vertes RP. Hippocampal theta rhythm: A tag for short-term memory. *Hippocampus*. 2005;15(7):923–935.
27. Mucke L, Masliah E, Yu G-Q, et al. High-level neuronal expression of Aβ 1–42 in wild-type human amyloid protein precursor transgenic mice: Synaptotoxicity without plaque formation. *J Neurosci*. 2000;20(11):4050–4058.
28. Vega-Flores G, Rubio SE, Jurado-Parras MT, et al. The GABAergic septohippocampal pathway is directly involved in internal processes related to operant reward learning. *Cereb Cortex*. 2014; 24(8):2093–2107.
29. Lim F, Hernández F, Lucas JJ, Gómez-Ramos P, Morán MA, Avila J. FTDP-17 mutations in tau transgenic mice provoke lysosomal abnormalities and tau filaments in forebrain. *Mol Cell Neurosci*. 2001;18(6):702–714.
30. Soler H, Dorca-Arévalo J, González M, et al. The GABAergic septohippocampal connection is impaired in a mouse model of tauopathy. *Neurobiol Aging*. 2017;49:40–51.
31. García-Cabrero AM, Guerrero-López R, Giráldez BG, et al. Hyperexcitability and epileptic seizures in a model of frontotemporal dementia. *Neurobiol Dis*. 2013;58:200–208.
32. Bjorklund NL, Reese LC, Sadagoparamanujam VM, Ghirardi V, Woltjer RL, Taglialatela G. Absence of amyloid β oligomers at the postsynapse and regulated synaptic Zn2 + in cognitively intact aged individuals with Alzheimer's disease neuropathology. *Mol Neurodegener*. 2012;7(1):23.
33. Briley D, Ghirardi V, Woltjer R, et al. Preserved neurogenesis in non-demented individuals with AD neuropathology. *Sci Rep*. 2016;6(1):27812.
34. Erten-Lyons D, Woltjer RL, Dodge H, et al. Factors associated with resistance to dementia despite high Alzheimer disease pathology. *Neurology*. 2009;72(4):354–360.
35. Iacono D, O'Brien R, Resnick SM, et al. Neuronal hypertrophy in asymptomatic Alzheimer disease. *J Neuropathol Exp Neurol*. 2008; 67(6):578–589.
36. Singh A, Allen D, Fracassi A, et al. Functional integrity of synapses in the central nervous system of cognitively intact individuals with high Alzheimer's disease neuropathology is associated with absence of synaptic tau oligomers. *J Alzheimer's Dis*. 2020; 78(4):1661–1678.
37. Zolochevska O, Bjorklund N, Woltjer R, Wiktorowicz JE, Taglialatela G. Postsynaptic proteome of non-demented individuals with Alzheimer's disease neuropathology. *J Alzheimer's Dis*. 2018;65(2):659–682.
38. Perez-Nievas BG, Stein TD, Tai H-C, et al. Dissecting phenotypic traits linked to human resilience to Alzheimer's pathology. *Brain*. 2013;136(Pt 8):2510–2526.
39. Barroeta-Espar I, Weinstock LD, Perez-Nievas BG, et al. Distinct cytokine profiles in human brains resilient to Alzheimer's pathology. *Neurobiol Dis*. 2019;121:327–337.
40. Paxinos G, Franklin KBJ. *The mouse brain in stereotaxic coordinates*. 2nd edn. Academic Press; 2001. doi:10.1016/S0306-453 0(03)00088-X
41. Pascual M, Pérez-Sust P, Soriano E. The GABAergic septohippocampal pathway in control and Reeler mice: Target specificity and termination onto reelin-expressing interneurons. *Mol Cell Neurosci*. 2004;25(4):679–691.
42. Schindelin J, Arganda-Carreras I, Frise E, et al. Fiji: An open-source platform for biological-image analysis. *Nat Methods*. 2012;9(7):676–682.
43. Arganda-Carreras I, Kaynig V, Rueden C, et al. Trainable Weka segmentation: A machine learning tool for microscopy pixel classification. *Bioinformatics*. 2017;33(15):2424–2426.
44. Gruart A, Muñoz MD, Delgado-García JM. Involvement of the CA3-CA1 synapse in the acquisition of associative learning in behaving mice. *J Neurosci*. 2006;26(4):1077–1087.
45. Múnera A, Gruart A, Muñoz MD, Delgado-Garcı'a JM. Scopolamine impairs information processing in the hippocampus and performance of a learned eyeblink response in alert cats. *Neurosci Lett*. 2000;292(1):33–36.
46. Fernández-Lamo I, Sánchez-Campusano R, Gruart A, Delgado-García JM. Functional states of rat cortical circuits during the unpredictable availability of a reward-related cue. *Sci Rep*. 2016; 6.37650.
47. Puighermanal E, Marsicano G, Busquets-Garcia A, Lutz B, Maldonado R, Ozaita A. Cannabinoid modulation of hippocampal long-term memory is mediated by mTOR signaling. *Nat Neurosci*. 2009;12(9):1152–1158.
48. Cissé M, Sanchez PE, Kim DH, Ho K, Yu GQ, Mucke L. Ablation of cellular prion protein does not ameliorate abnormal neural network activity or cognitive dysfunction in the J20 line of human amyloid precursor protein transgenic mice. *J Neurosci*. 2011; 31(29):10427–10431.
49. Harris JA, Devidze N, Halabisky B, et al. Many neuronal and behavioral impairments in transgenic mouse models of Alzheimer's disease are independent of caspase cleavage of the amyloid precursor protein. *J Neurosci*. 2010;30(1):372–381.
50. Navarro P, Guerrero R, Gallego E, et al. Memory and exploratory impairment in mice that lack the Park-2 gene and that over-express the human FTDP-17 mutant Tau. *Behav Brain Res*. 2008; 189(2):350–356.
51. Jin M, Shepardson N, Yang T, Chen G, Walsh D, Selkoe DJ. Soluble amyloid beta-protein dimers isolated from Alzheimer cortex directly induce Tau hyperphosphorylation and neuritic degeneration. *Proc Natl Acad Sci U S A*. 2011;108(14):5819–5824.
52. Zempel H, Thies E, Mandelkow E, Mandelkow E-M. Aβ oligomers cause localized Ca^{2+} elevation, missorting of endogenous Tau

into dendrites, Tau phosphorylation, and destruction of microtubules and spines. *J Neurosci*. 2010;30(36):11938–11950.
53. Ittner A, Chua SW, Bertz J, et al. Site-specific phosphorylation of tau inhibits amyloid-β toxicity in Alzheimer's mice. *Science*. 2016;354(6314):904–908.
54. Dávila-Bouziguet E, Targa-Fabra G, Ávila J, Soriano E, Pascual M. Differential accumulation of Tau phosphorylated at residues Thr231, Ser262 and Thr205 in hippocampal interneurons and its modulation by Tau mutations (VLW) and amyloid-β peptide. *Neurobiol Dis*. 2019;125:232–244.
55. Blazquez-Llorca L, Garcia-Marin V, DeFelipe J. Pericellular innervation of neurons expressing abnormally hyperphosphorylated tau in the hippocampal formation of Alzheimer's disease patients. *Front Neuroanat*. 2010;4:20.
56. Angulo SL, Orman R, Neymotin SA, et al. Tau and amyloid-related pathologies in the entorhinal cortex have divergent effects in the hippocampal circuit. *Neurobiol Dis*. 2017;108:261–276.
57. Busche MA, Wegmann S, Dujardin S, et al. Tau impairs neural circuits, dominating amyloid-β effects, in Alzheimer models in vivo. *Nat Neurosci*. 2019;22(1):57–64.
58. Roberson ED, Scearce-Levie K, Palop JJ, et al. Reducing endogenous tau ameliorates amyloid β-induced deficits in an Alzheimer's disease mouse model. *Science*. 2007;316(5825):750–754.
59. Roberson ED, Halabisky B, Yoo JW, et al. Amyloid-β/Fyn-induced synaptic, network, and cognitive impairments depend on tau levels in multiple mouse models of Alzheimer's disease. *J Neurosci*. 2011;31(2):700–711.
60. Bolmont T, Clavaguera F, Meyer-Luehmann M, et al. Induction of Tau pathology by intracerebral infusion of amyloid-β-containing brain extract and by amyloid-β deposition in APP × Tau transgenic mice. *Am J Pathol*. 2007;171(6):2012–2020.
61. Lewis J, Dickson DW, Lin WL, et al. Enhanced neurofibrillary degeneration in transgenic mice expressing mutant tau and APP. *Science*. 2001;293(5534):1487–1491.
62. Ribé EM, Pérez M, Puig B, et al. Accelerated amyloid deposition, neurofibrillary degeneration and neuronal loss in double mutant APP/tau transgenic mice. *Neurobiol Dis*. 2005;20(3):814–822.
63. Götz J, Chen F, van Dorpe J, Nitsch RM. Formation of neurofibrillary tangles in P301L tau transgenic mice induced by Aβ42 fibrils. *Science*. 2001;293(5534):1491–1495.
64. Nisbet RM, Polanco J-C, Ittner LM, Götz J. Tau aggregation and its interplay with amyloid-β. *Acta Neuropathol*. 2015;129(2):207–220.
65. Pérez M, Ribe E, Rubio A, et al. Characterization of a double (amyloid precursor protein-tau) transgenic: Tau phosphorylation and aggregation. *Neuroscience*. 2005;130(2):339–347.
66. Götz J, Probst A, Spillantini MG, et al. Somatodendritic localization and hyperphosphorylation of tau protein in transgenic mice expressing the longest human brain tau isoform. *Embo J*. 1995;14(7):1304–1313.
67. Rossi D, Gruart A, Contreras-Murillo G, et al. Reelin reverts biochemical, physiological and cognitive alterations in mouse models of Tauopathy. *Prog Neurobiol*. 2020;186:101743.
68. Ando K, Maruko-Otake A, Ohtake Y, Hayashishita M, Sekiya M, Iijima KM. Stabilization of microtubule-unbound tau via tau phosphorylation at Ser262/356 by Par-1/MARK contributes to augmentation of AD-related phosphorylation and Aβ42-induced tau toxicity. *PLoS Genet*. 2016;12(3):e1005917.
69. Palop JJ, Mucke L. Amyloid-β–induced neuronal dysfunction in Alzheimer's disease: From synapses toward neural networks. *Nat Neurosci*. 2010;13(7):812–818.
70. Essrich C, Lorez M, Benson JA, Fritschy J-M, Lüscher B. Postsynaptic clustering of major GABAA receptor subtypes requires the γ2 subunit and gephyrin. *Nat Neurosci*. 1998;1(7):563–571.
71. Maric HM, Hausrat TJ, Neubert F, et al. Gephyrin-binding peptides visualize postsynaptic sites and modulate neurotransmission. *Nat Chem Biol*. 2017;13(2):153–160.
72. Tyagarajan SK, Ghosh H, Yévenes GE, et al. Regulation of GABAergic synapse formation and plasticity by GSK3β-dependent phosphorylation of gephyrin. *Proc Natl Acad Sci U S A*. 2011;108(1):379–384.
73. Tyagarajan SK, Fritschy J-M. Gephyrin: A master regulator of neuronal function? *Nat Rev Neurosci*. 2014;15(3):141–156.
74. Colom LV, Castañeda MT, Bañuelos C, et al. Medial septal β-amyloid 1-40 injections alter septo-hippocampal anatomy and function. *Neurobiol Aging*. 2010;31(1):46–57.
75. Özdemir MB, Erdogan C, Iwasaki K, Watanabe T, Ishikane S, Fujiwara M. Injection of specific amyloid-beta oligomers (beta 1-40:beta 1-42 = 10:1) into rat medial septum impairs memory retention without inducing hippocampal apoptosis. *Neurol Res*. 2013;35(8):798–803.
76. Villette V, Poindessous-Jazat F, Simon A, et al. Decreased rhythmic GABAergic septal activity and memory-associated oscillations after hippocampal amyloid- pathology in the rat. *J Neurosci*. 2010;30(33):10991–11003.
77. Cullen KM, Halliday GM, Double KL, Brooks WS, Creasey H, Broe GA. Cell loss in the nucleus basalis is related to regional cortical atrophy in Alzheimer's disease. *Neuroscience*. 1997;78(3):641–652.
78. Kerbler GM, Fripp J, Rowe CC, et al.; Alzheimer's Disease Neuroimaging Initiative. Basal forebrain atrophy correlates with amyloid β burden in Alzheimer's disease. *NeuroImage Clin*. 2015;7:105–113.
79. Cantero JL, Atienza M, Lage C, et al.; Alzheimer's Disease Neuroimaging Initiative. Atrophy of basal forebrain initiates with tau pathology in individuals at risk for Alzheimer's disease. *Cereb Cortex*. 2020;30(4):2083–2098.
80. Vogels OJM, Broere CAJ, Ter Laak HJ, Ten Donkelaar HJ, Nieuwenhuys R, Schulte BPM. Cell loss and shrinkage in the nucleus basalis Meynert complex in Alzheimer's disease. *Neurobiol Aging*. 1990;11(1):3–13.